THE CORRELATED X-RAY AND OPTICAL TIME VARIABILITY OF TT ARIETIS

K. A. JENSEN,[1] FRANCE A. CÓRDOVA,[2] AND J. MIDDLEDITCH
University of California, Los Alamos National Laboratory

KEITH O. MASON[2]
University College London; Mullard Space Science Laboratory

A. D. GRAUER[3]
Louisiana State University Observatory, Louisiana State University

AND

KEITH HORNE AND RICHARD GOMER[4]
Hale Observatories,[5] California Institute of Technology
Received 1982 October 11; accepted 1982 December 10

ABSTRACT

Simultaneous X-ray and optical photometry of the cataclysmic variable TT Arietis has revealed correlated X-ray and optical variability over a broad range of time scales. Large amplitude X-ray flickering with a time scale of ~ 1000 s persists for the entire observation, is present at all orbital phases, and is correlated with optical flickering. The X-ray flickering is delayed by ~ 1 minute with respect to the optical flickering. Transient hard X-ray oscillations with periods ~ 32 s, ~ 12 s, and ~ 9 s and transient optical oscillations with periods ~ 32 s and ~ 12 s are observed. There is a modulation of the X-ray flux with a period consistent with the orbital period of approximately 200 minutes, but there is no apparent modulation of the X-ray spectrum. The optical flux is modulated with a similar period and may lag the X-ray modulation by ~ 0.1 in phase. An X-ray photoelectric absorption event with a duration of about 1000 s is observed. An optical flux decrease of shorter duration (~ 500 s) occurs at the same time. The X-ray spectrum is well fitted by a thermal bremsstrahlung plus Gaunt factor model with $kT \gtrsim 10$ keV, $N_H = 1-2 \times 10^{21}$ cm^{-2}, and a received flux of $\sim 2 \times 10^{-11}$ ergs cm^{-2} s^{-1} between 0.2 and 4 keV. The results of our observations suggest that the hard X-ray emission from TT Ari may be produced in a corona above and below the inner accretion disk.

Subject headings: radiation mechanisms — stars: dwarf novae — stars: individual — X-rays: binaries

I. INTRODUCTION

TT Arietis (BD $+14°341$) has been classified as a nova-like variable because of the similarity of its spectrum and photometric variability to those of the novae. In these systems, a red dwarf is presumed to fill its Roche lobe and transfer mass to a white dwarf companion. Cowley et al. (1975) suggested an orbital period for the system of 0^d13755 based on optical radial velocity measurements. However, this period does not fit the optical photometric modulation of the star very well (cf. Smak and Stępień 1975), so that the exact period is still in doubt. The optical brightness of TT Ari varies irregularly on long time scales: during the 50 years prior to 1980 November it was reported at visual magnitudes between 9.5 and 12, but since that time it has been observed at magnitudes as faint as 16 (Krautter et al. 1981a; Mattei and Bortle 1982; Shafter et al. 1982). Rapid quasi-coherent optical variations have been observed in TT Ari

on time scales of 800–1000 s (Williams 1966; Smak and Stępień 1969; and Mardirossian et al. 1980), and ~ 40 s (Mardirossian et al. 1980).

A short X-ray observation of TT Ari using the *Einstein* X-ray satellite showed it to be a hard X-ray source (Córdova, Mason, and Nelson 1981), with a flux of 1.4×10^{-11} ergs cm^{-2} s^{-1} in the 0.15–4.5 keV band, assuming a temperature of 10 keV and a column density of 10^{20} cm^{-2}. In this paper, we report the results of a longer follow-up *Einstein* X-ray observation, and simultaneous optical observations, extending over several binary orbits. We find evidence for correlations between the X-ray and optical variability of TT Ari on three distinct time scales: the 3.3 hour variability that has been associated with the orbital period of the star; the ~ 1000 s time scale of the irregular flickering activity; and the time scale of quasi-coherent oscillations which have periods of order 10 s.

II. OBSERVATIONS

TT Ari was observed on 1980 July 19 and 20 with the Imaging Proportional Counter (IPC) and the Monitor Proportional Counter (MPC) on the *Einstein* X-ray satellite (Giacconi et al. 1979) for a total effective

---

exposure time on the source of 24,000 s. The IPC data were collected in 32 pulse height (PHA) channels covering the energy range 0.15–4.5 keV; the temporal resolution of this instrument was 1 ms, and the spatial resolution was about 1′. The MPC, which was not an imaging intrument and therefore had a large background signal, covered the energy range 2–18 keV. For the spectral analysis described here, data from both detectors were used, but for the timing analysis only the IPC data were used.

Simultaneous optical observations were made during both nights by A. G. at the Louisiana State University (LSU) Observatory and by K. H. and R. G. at the Mount Wilson (MTW) Observatory. The LSU data were obtained with a two-star photometer. A thorough discussion of the instrument, observing techniques, and examples of its operation has been published by Grauer and Bond (1981). Standard *B* filters and 2 s integrations were used. The MTW data were obtained with a single channel S-20 photometer on the 1.5 m telescope. A broad-band (1900 Å FWHM) filter with peak response near 4500 Å was employed. Photon counts were recorded in 0.1 s integrations. An absolute timing accuracy of 5 ms was achieved for LSU and MTW data by reference to WWV broadcasts. The LSU and MTW data are $\sim 100\%$ correlated in time intervals where they overlap, indicating that there is no significant difference in the response of the two instruments to the variability of TT Ari and that any time offset between the two sets of data is smaller than 2 s.

The journal of observations is given in Table 1. The X-ray data consist of discrete sets of approximately 3100 s duration, separated by gaps of approximately 2500 s during which the source was occulted by the Earth. Each discrete set of X-ray data is labeled with a (satellite) orbit number. Simultaneous optical coverage was obtained for 75% of the X-ray observation.

TABLE 1

JOURNAL OF OBSERVATIONS

DATE	UT (s)		
	Einstein	LSU	MTW
1980 July 19	OB0: 20616–21058		
	OB1: 23598–26661		
	OB2: 29244–32350	26524–35298	34907–43226
	OB3: 34917–37994		
	OB4: 40532–43027		
1980 July 20	OB5: 21917–24984		
	OB6: 27529–30601		
	OB7: 33168–36274	27319–36537	33486–42473
	OB8: 38812–41878		

III. RESULTS

a) The X-Ray Spectrum

From least squares fits of thermal bremsstrahlung plus Gaunt factor model spectra to six pulse height (PHA) channels of MPC data covering the range 2–10 keV, we find that kT is $\gtrsim 10$ keV and the received flux is $\sim 2.5 \times 10^{-11}$ ergs cm^{-2} s^{-1} in the 2–10 keV band. Using IPC data which cover the energy interval 0.2–4.0 keV, and fixing the temperature to be ≥ 10 keV, column densities in the range $(1–2) \times 10^{21}$ cm^{-2} and a received flux of $\sim 2 \times 10^{-11}$ ergs cm^{-2} s^{-1} in the 0.2–4.0 keV band are derived. The uncertainty in the column density is dominated by our lack of knowledge of the precise detector gain.

b) Orbital Modulation

The optical light curves are shown in Figure 1. Normalization of the data from the two observatories was checked by comparing the intensities during a 2500 s overlap period on July 20. An intensity of 10^4 counts s^{-1} corresponds to a received flux of $\sim 5 \times 10^{-25}$ ergs cm^{-2}
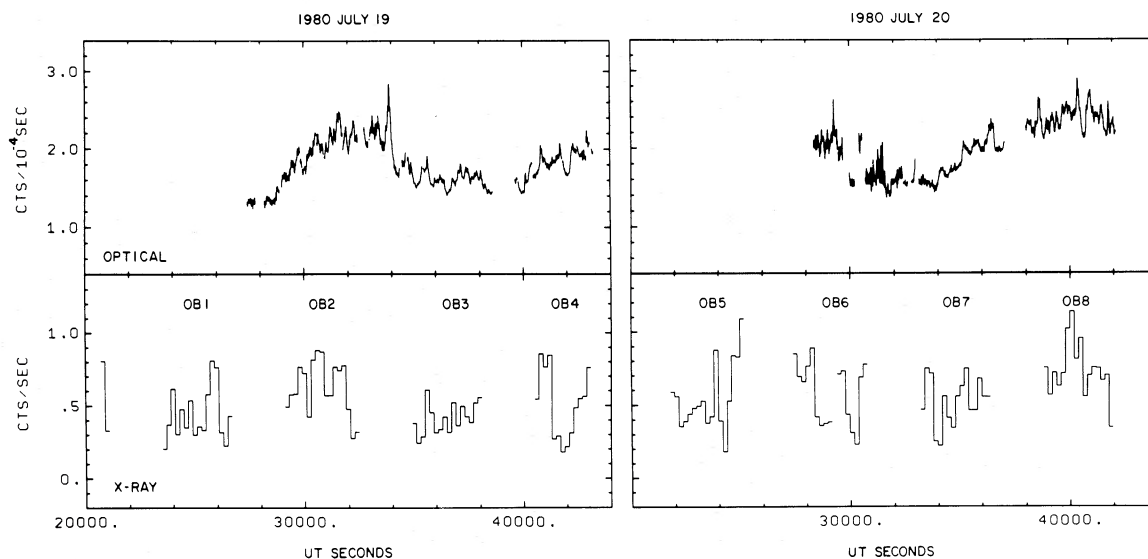

FIG. 1.—Optical and X-ray light curves for 1980 July 19 and 1980 July 20. The *Einstein* satellite orbit numbers corresponding to the X-ray data are indicated.

s⁻¹ Hz⁻¹ in the blue band. The X-ray light curves are also shown in Figure 1; the bin size is 200 s. The periodic satellite occultation gaps are evident.

The optical light curves show a roughly sinusoidal variation in the intensity between *B* magnitudes 11.5 and 11.9 over a period of ~12,000 s. No *V* magnitudes are available for the time of these observations, but in early September of 1980 a visual light curve also displaying an approximately sinusoidal variation between 11.5 and 12.0 mag was obtained by the authors, using the FES on the *International Ultraviolet Explorer* satellite, and, a few days later, in *B* light, with the Shane telescope and Image Dissection Scanner of the Lick Observatory. There is evidence of a similar modulation in the X-ray data. The optical modulation is known from previous observations (e.g., Mardirossian *et al.* 1980) and is attributed to a binary orbital effect. The orbital period of TT Ari is not well established. Cowley *et al.* (1975) derived a period of 0.13755 days from the radial velocities of Balmer emission lines. Smak and Stępień (1975) have contended that their photometric observations spaced months apart are more compatible with a period of ~0.1329 days, though noting that there may not be a stable photometric period.

In Figure 2, we present the very low frequency power spectra for the entire X-ray and optical data sets, illustrating variability on the time scale of the binary modulation. The mean fluxes for the two nights were normalized to remove the effects of variability on time scales ≳1 day. Data gaps equivalent to the X-ray satellite occultation gaps were added to the optical data

so that any effects due to aliasing would be reflected equally in both power spectra. All data gaps have been padded with the average count rate. The raw power spectra were smoothed over 0.0244 mHz to remove the fine scale aliasing caused by the occultation gaps and the large gap between the two nights. The X-ray and optical power spectra are similar in shape at frequencies less than 0.1 mHz where power due to an orbital modulation is expected. The features near ~0.23 mHz are beats between the satellite period and the observation lengths for each night. The many features in the X-ray spectrum between 0.3 and 1.0 mHz are caused by flickering (see § IIIc). They are also present in the optical power spectrum, but at a lower amplitude relative to the power near the orbital frequency.

The optical and X-ray data are folded modulo (40 bins per period) the spectroscopic period of 0.13755 days and Smak and Stępień's photometric period of 0.1329 days in Figure 3. Also shown is an X-ray spectral indicator, a hardness ratio (HR) defined as the ratio of counts that appear above and below 1.0 keV in the IPC pulse height data. Phase 0.0 is defined as UT 20616 s on 1980 July 19, corresponding to the beginning of the *Einstein* observation. The optical and X-ray fluxes both show a quasi-sinusoidal variation. We plot each data point twice, displaced by one cycle, to illustrate the modulation more clearly.

Because of the prominent flickering in the X-ray data, it is more difficult to derive a folded X-ray light curve that shows only the orbital trend. We have attempted to ascertain the effects of the flickering by the following
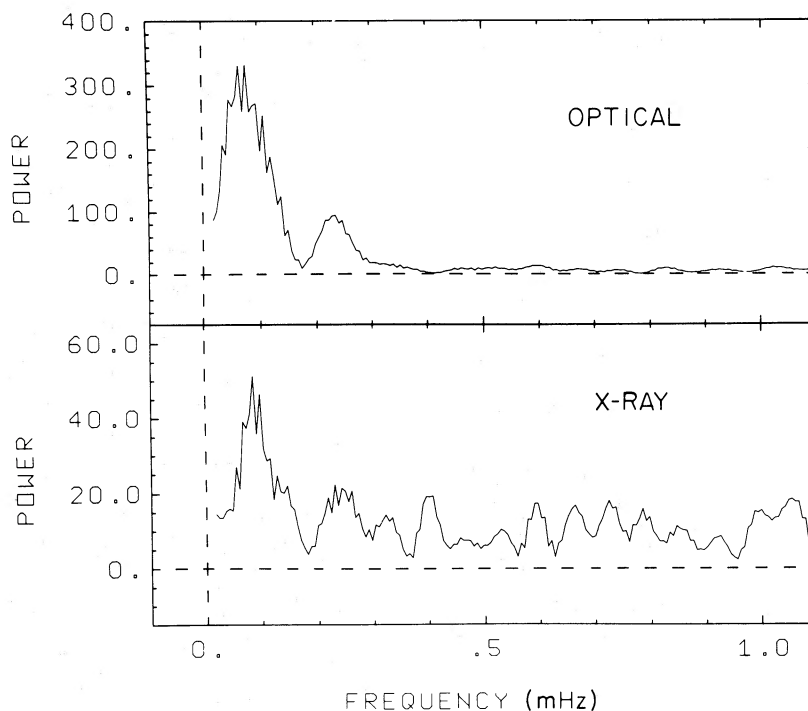

FIG. 2.—Optical and X-ray very low frequency power spectra, illustrating variability on the time scale of the binary modulation
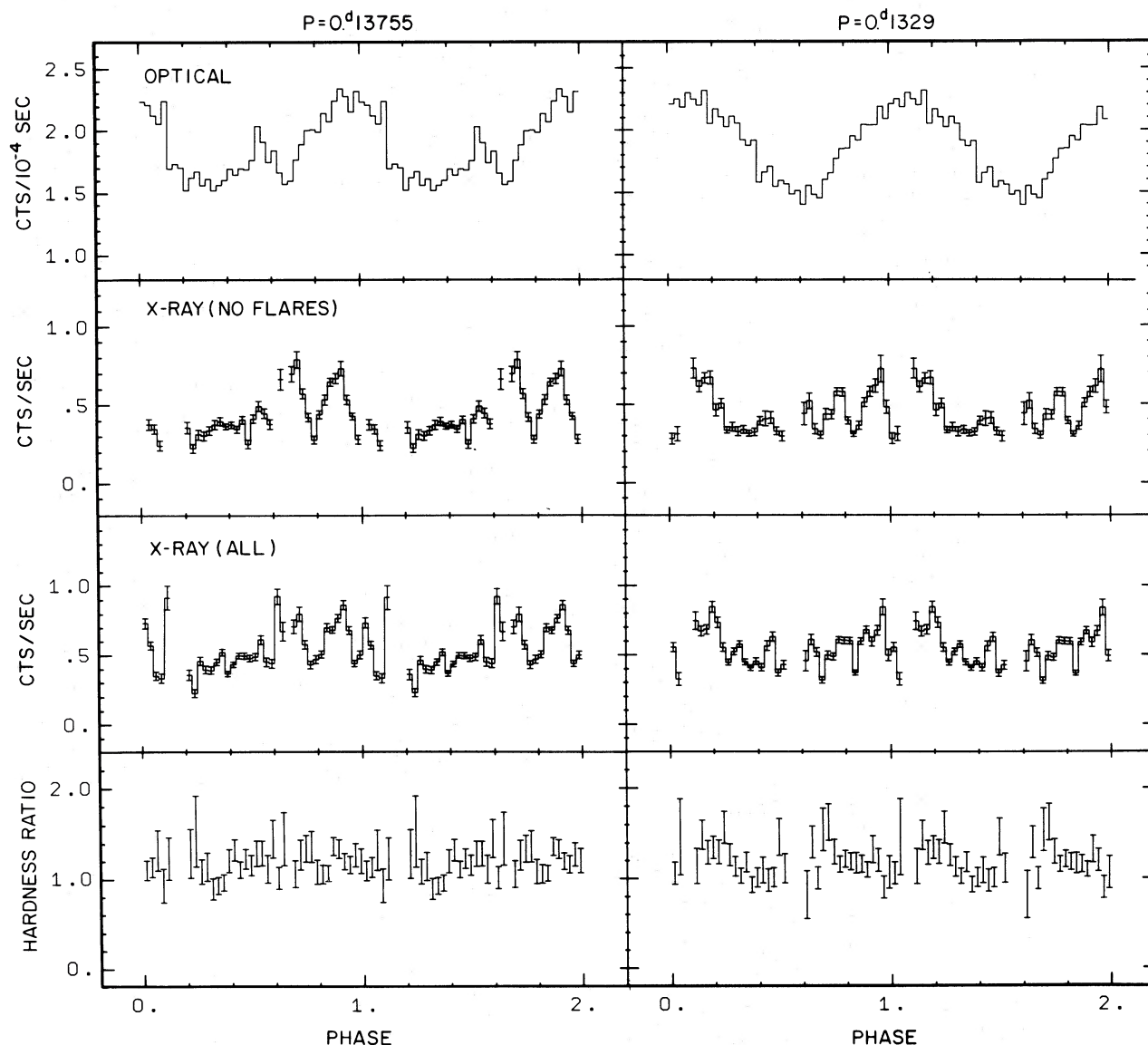
FIG. 3.—Optical and X-ray data folded modulo the spectroscopic (0^d13755) and photometric (0^d1329) periods (40 bins per period). Two cycles are shown.

procedure. The light curves for each of the satellite orbits were examined by eye, and prominent X-ray flares were identified. Two X-ray data sets were created. One set contains all of the data. In the other set, the data covering times of prominent flaring were removed. All analysis of X-ray variability on time scales longer than the flickering time scales was conducted on each data set separately. When the results of the analyses of the separate data sets differ by an amount greater than their formal uncertainties, we consider the actual uncertainties in our analysis to be dominated by these differences.

Modulation of the X-ray flux on the orbital period is evident in each case. There appears to be a constant minimum X-ray flux for approximately half of the orbit

during which the count rate is 50%–60% of the peak. Modulation of the hardness ratio is not evident, indicating that there is no detectable orbital modulation of the X-ray spectrum.

There appears to be a secondary X-ray flux minimum during the high intensity phases. This minimum is caused by a large decrease in the X-ray flux during orbit 4 on July 19 between UT 41300 s and UT 42300 s. There is also a decrease in the optical flux between UT 41800 s and UT 42300 s (Fig. 4). The most convincing evidence that this event is not simply a quiescent period between flares is the hardening of the X-ray spectrum during this time. In Figure 5, the hardness ratio is shown for X-ray data collected in 600 s bins. The anomalously high hardness ratio corresponds to UT 41500–42100 s
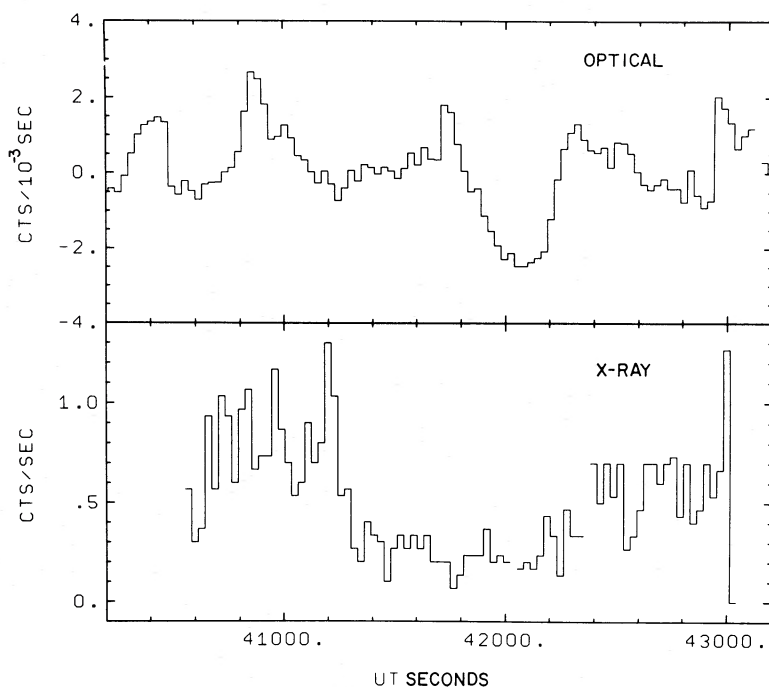
FIG. 4.—Optical and X-ray light curves for orbit 4. The bin size is 30 s. The optical data are residuals from a cubic fit.

and coincides with the flux decrease. An examination of the PHA distribution during the event shows that the flux decrease is due to a deficiency of photons in PHA channels corresponding to 0.2–1.0 keV, suggesting that photoelectric absorption was probably responsible for the decrease. There is no evidence to suggest that the occurrence of the absorption event is related to the orbital phase since it is not seen on the previous cycle (orbit 2).

To examine the correlation between the orbital modulations in the X-ray and optical bands, eight cross

correlation functions (CCFs) were calculated, in which the data were treated in different ways. Table 2 lists the data sets correlated and the results for each of these CCFs. The calculation of these CCFs followed the prescription of Weisskopf, Kahn, and Sutherland (1975). Four functions were required to accomodate the two possible periods and the two X-ray data sets (with and without the flares). Four additional functions were calculated with the data of orbit 4 excluded. This was done because the absorption event during orbit 4 may have been anomalous.
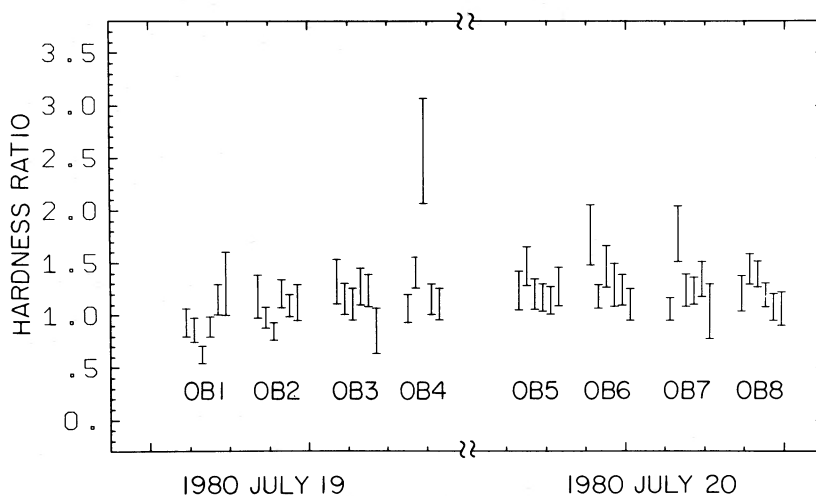
FIG. 5.—X-ray hardness ratios for all IPC data. Each point represents 600 s of data. The corresponding satellite orbit numbers are indicated.

TABLE 2

CROSS CORRELATION ANALYSIS OF THE ORBITAL MODULATION

Case	Period (days)	X-Ray Data Set	CCF	Optical Phase Lag
1.....	0.13755	All data	0.45	0.070 ± 0.009
2.....	0.1329	All data	0.44	0.069 ± 0.011
3.....	0.13755	Flares excluded	0.62	0.130 ± 0.007
4.....	0.1329	Flares excluded	0.48	0.119 ± 0.011
5.....	0.13755	OB4 excluded	0.56	0.073 ± 0.007
6.....	0.1329	OB4 excluded	0.48	0.085 ± 0.009
7.....	0.13755	Flares and OB4 excluded	0.75	0.109 ± 0.007
8.....	0.1329	Flares and OB4 excluded	0.46	0.109 ± 0.012

Mean lag plus error: All eight functions:	0.0970 ± 0.0230
Mean lag plus error: Spectroscopic period:	0.0982 ± 0.0246
Mean lag plus error: Photometric period:	0.0946 ± 0.0191
Mean lag plus error: All data:	0.0742 ± 0.0061
Mean lag plus error: Flares removed:	0.1174 ± 0.0094

The results of the cross-correlation analysis are summarized in Table 2. In each case, there is a correlation between the folded X-ray and optical intensities and the optical curve lags the X-ray curve. This effect is illustrated in Figure 6, which shows the CCF for case 7, the case with the strongest correlation. The lag is determined by finding the weighted center of the CCF. The formal uncertainty in the lag is determined by propagation of errors in the weighted sums. Inspection of Table 2 indicates that the scatter in the derived lags for the various CCFs is greater than would be expected from the formal uncertainties, suggesting that the uncertain period and uncertainties due to flaring and absorption events determine the actual error in the measurement of a phase lag. To estimate this error, we calculated the standard deviation in the scatter of the eight derived lags. The resulting mean lag plus error is 0.10 ± 0.02. Since there are only a small number of cases which are not mutually independent, it is possible that we are underestimating the uncertainty in the phase lag.

c) Flickering

Figure 1 shows ~ 0.2 mag optical flickering on time scales of several minutes, similar to the variability observed by Williams (1966), Smak and Stępień (1969), and Mardirossian *et al.* (1980). Flickering is also present in the X-ray data. In Figure 7 we present optical and X-ray data obtained simultaneously during orbit 2. The data are residuals from a cubic fit, integrated into 30 s bins. Three X-ray flares are prominent, with amplitudes of a factor of 2–3 times the residual intensity and durations of 150–600 s. Associated flares can be seen in the optical data. X-ray and optical flickering occur during every orbit and at all orbital phases.

In Figure 8 we present X-ray and optical low-frequency power spectra, illustrating variability on flickering time scales. The power spectra are similar. Both are dominated
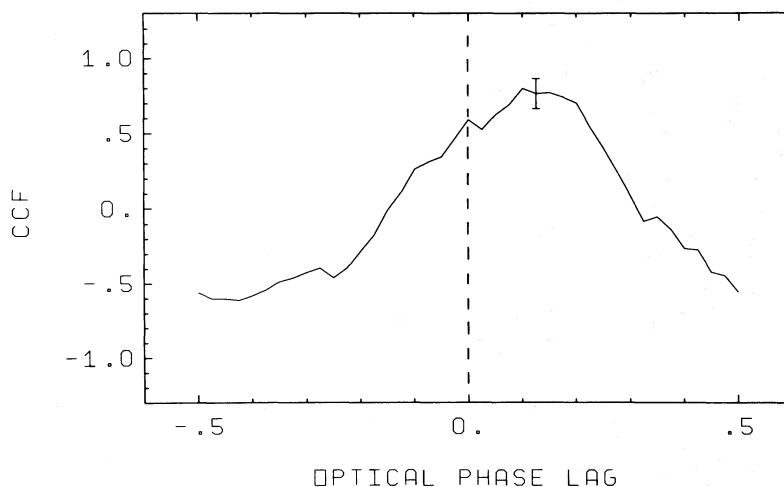

FIG. 6.—Cross-correlation function for the optical and X-ray folded light curves for case 7 (cf. Table 2), where a 0^d13755 period was used and flares and orbit 4 were removed from the X-ray data.
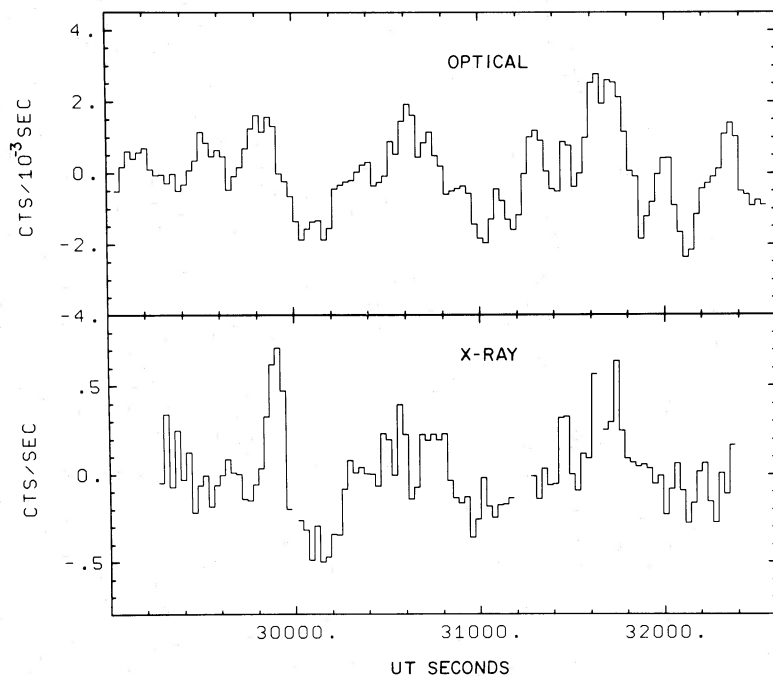
FIG. 7.—Optical and X-ray light curves for orbit 2. The bin size is 30 s. The data are residuals from cubic fits.
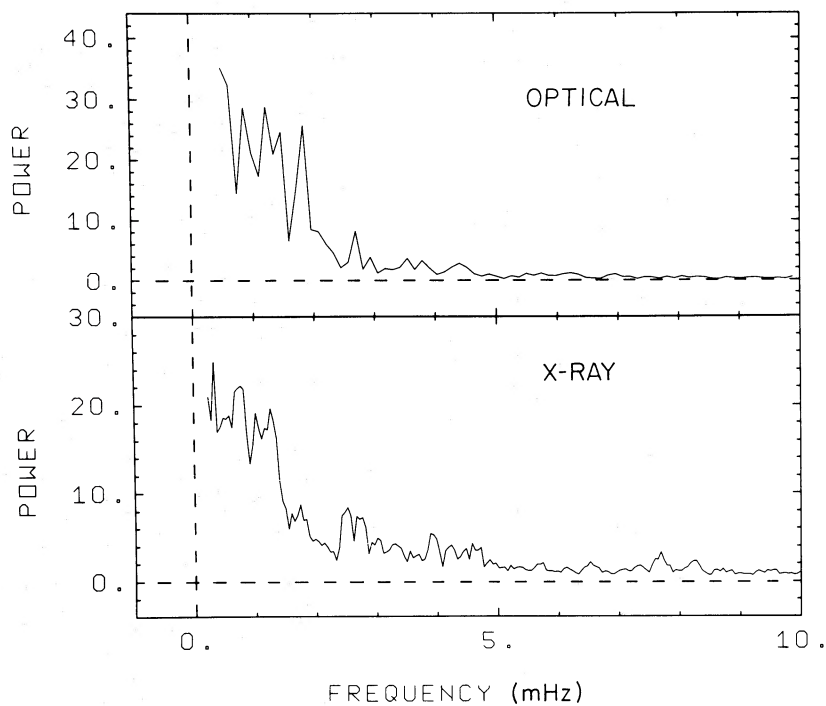
FIG. 8.—Optical and X-ray low frequency power spectra, illustrating variability on flickering time scales

TABLE 3

AUTOCORRELATION ANALYSIS OF THE FLICKERING

OB	Optical Observer	t_z (s)				
		(Optical)	(0.2–4.0 keV)	(1.0–4.0 keV)	(0.2–1.0 keV)	(0.2–0.5 keV)
1	None	...	264 ± 24	313 ± 67	241 ± 30	205 ± 92
2	LSU	174	153 ± 28	197 ± 50	124 ± 40	184 ± 69
3	MTW	393	137 ± 20	...	140 ± 38	...
4	MTW	190	184 ± 23	151 ± 41	171 ± 31	...
5	None	...	205 ± 12	193 ± 20	190 ± 21	201 ± 76
6	LSU	229	251 ± 20	198 ± 45	280 ± 26	262 ± 85
7	LSU	224	204 ± 18	159 ± 26	218 ± 23	...
8	MTW	144	152 ± 33	239 ± 103	114 ± 46	...
All	...	...	209 ± 10	205 ± 25	200 ± 14	197 ± 46
All except 4 ...	...	...	205 ± 9	202 ± 21	198 ± 13	205 ± 38
2, 3, 4, 6, 7, 8..	Both	195	199 ± 16	192 ± 50	193 ± 19	191 ± 57
2, 3, 6, 7, 8	Both	196	192 ± 14	188 ± 36	190 ± 18	206 ± 49

by power at frequencies less than 2 mHz. From the broad distribution of power over this frequency range, it can be seen that the flickering is not a strictly periodic phenomenon.

Additional information on the nature of the flickering can be obtained from autocorrelation functions (ACFs). ACFs were calculated for X-ray data sets corresponding to each of the *Einstein* orbits and for simultaneous optical data sets. Each data set consists of ∼300 10 s bins. To minimize the effects of orbital modulation, a cubic trend was removed from each set. To analyze the spectral characteristics of the X-ray flickering, the X-ray data were separated into broad energy bands and ACFs were calculated for each band. LSU and MTW data were separated for the calculation of optical ACFs. ACFs and CCFs for the flickering were computed from the prescription of Weisskopf, Kahn, and Sutherland (1975).

The results of the autocorrelation analysis for the individual orbits are presented in Table 3. For each orbit, we have calculated the ACF zero crossing time (t_z). The value of the t_z is sensitive to the manner in which the data are detrended. Successively higher order polynomial detrending will tend to remove correlations on successively shorter time scales, thereby reducing t_z. Our simulations suggest that a cubic fit optimizes the removal of orbital trends while preserving the flickering. Table 3 shows that t_z is different for different orbits, but that there is no significant difference between X-ray and optical flickering time scales for any individual orbit except orbit 3. The characteristic time scales are also essentially the same for low-energy and high-energy X-ray data. The similarity of the X-ray and optical flickering is clear in Figure 9 which shows the ACF for all the simultaneous data.

To investigate whether the X-ray and optical flickering are correlated, cross-correlation functions were calculated for each simultaneous orbit. The CCFs are shown in Figure 10. The oscillations in these functions result from interference between adjacent flares. The largest peak for each orbit, except orbit 4, occurs near a lag of zero, suggesting that this peak represents the

true correlation time scale. To obtain a clearer indication of the correlation, a CCF was calculated for all simultaneous data. Because the recurrence rates of the flares vary from orbit to orbit, those features in the CCFs for the individual orbits due to coincidental placement of unrelated flares will tend to vanish, while true correlations will be preserved. Figure 11 shows the CCF for all data from orbits 2, 3, 6, 7, and 8. The correlation near zero lag persists. The side lobes approximately 1000 s from the main feature reflect a tendency for flares to recur after 1000 s. Orbit 4 was omitted because of its anomalous absorption event. Its inclusion has only a minor effect. The positive correlation near zero lag represents a persistent correlation between the optical and X-ray flickering.

In Table 4, we present the results of the cross-correlation analysis of the flickering. With the exception of the anomalous orbit 4, there is a time delay between the optical and X-ray flickering, with the X-ray flickering *lagging* the optical flickering. The average time delay is 58 s, and there appears to be significant scatter from orbit to orbit. The deviation of the CCFs from zero lag can be seen in Figures 10 and 11.

It is possible that some of the flickering is not correlated. The CCFs are all significantly less than 1.0 (see Table 4), suggesting that uncorrelated flickering occurs. If we assume that unrelated flares occur at random with respect to related flares, then on average the effects of uncorrelated flickering on the CCF lags should balance (positive and negative) so that the measured lag is a reliable estimate of the delay in the related flickering. However, there will be localized fluctuations in the effect which, for finite data sets, can result in a scatter in measured lags. Such an effect may be responsible for the orbit by orbit scatter in the lag. It is unlikely, however, that any error in the time lag will be larger than the 20 s standard deviation in the orbit by orbit scatter. It is not likely that the time calibration for the *Einstein* data is in error (Harnden 1982), so that the observed time delay of 60 ± 20 s between correlated optical and X-ray flares is a real effect.
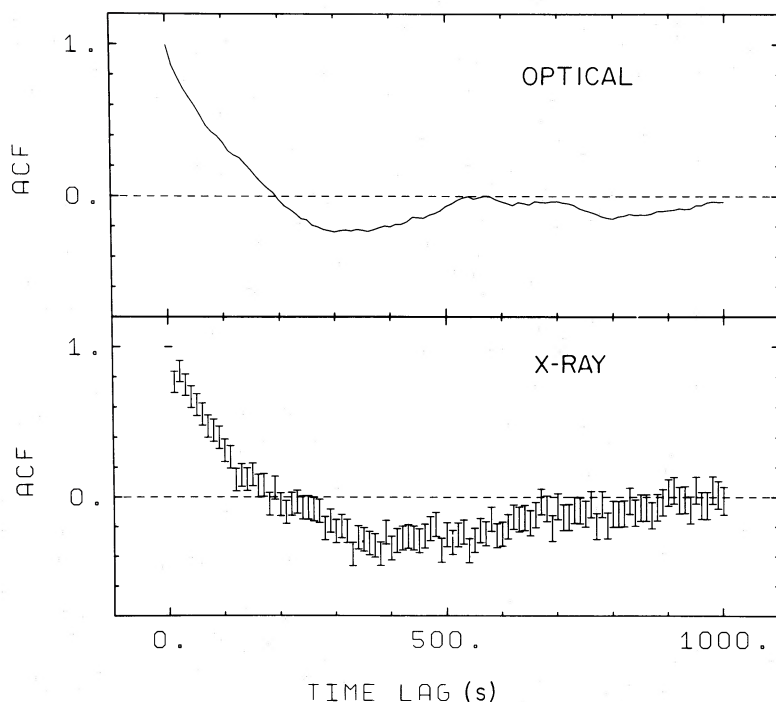
Fig. 9.—Optical and X-ray autocorrelation functions for all simultaneous data

Since the detrended power spectra are dominated by variance on flickering time scales, the ratio of the detrended X-ray and optical variance will be an accurate measure of the flickering flux ratio. In that case, we can compare the ratio of X-ray (0.2–4.0 keV) to optical (3700–5600 Å) luminosity in the flickering to the ratio in the total data:

$$(L_x/L_B)_{\text{total}} = K_t(I_x/I_B)$$

$$(L_x/L_B)_{\text{flickering}} = K_f(V_x/V_B)^{1/2} \, ,$$

where V_x and V_B are the count rate variance in the detrended X-ray and optical data, respectively; I_x and I_B are the average X-ray and optical count rate intensities; and K_t and K_f are relative X-ray/optical conversion factors from photon count rate to energy flux for the total data and the flickering. The conversion factor for the X-ray band was determined from spectral fits to all of the IPC data. From the comparative

hardness ratios of the total data and the flickering, we infer $K_t \sim K_f$. The X-ray variance is corrected to account for a Poisson contribution. The conversion factor for the optical band was determined by measurements of the reference star. From our measurements, we derive:

$$(L_x/L_B)_{\text{total}} = 0.1$$
$$(L_x/L_B)_{\text{flickering}} = 0.5 \, ,$$

confirming that flickering is more prominent in the X-ray band. Because of uncertainties in the determination of the conversion factors, each of these ratios is only accurate to about 50%, but the factor of 5 larger ratio for the flickering is not sensitive to these uncertainties and can be regarded as accurate to about 10%.

Since the variance measures the rms amplitude of the flickering, the ratio $(V_x)^{1/2}/I_x \sim 0.7$ shows that the flux in the X-ray flickering is 70%–100% of the total X-ray flux. The ratio $(V_B)^{1/2}/I_B \sim 0.15$ shows that the flux in the optical flickering is 15%–20% of the total optical flux.

d) Rapid Oscillations

In Figure 12, we present the power spectrum for run L2M, obtained at LSU on July 20 between UT 30393 s and UT 34489 s. The run consists of 2048 2 s bins, with a Nyquist frequency of 250 mHz and resolution of 0.244 mHz per bin. The power is normalized so that the average is unity and has been smoothed over three bins (0.73 mHz). A spectral feature is present at $f_0 \sim 80.6$ mHz (12.4 s); its power is spread out over several frequency bins. A feature also appears at $f_0 \sim 31.5$ mHz (31.7 s). Less conspicuous in this spectrum is a broader

TABLE 4

X-Ray/Optical Flickering Correlations

OB	CCF	Optical Time Lag (s)
2	0.68	-43 ± 3
3	0.43	-33 ± 7
4	...	...
6	0.55	-101 ± 6
7	0.52	-42 ± 4
8	0.57	-62 ± 4
1–8	0.46	-59 ± 2
1–8 (no 4)	0.50	-58 ± 2

region of enhanced power between 22 and 31 mHz. This corresponds to the range of the transient oscillations observed in TT Ari by Mardirossian *et al.* (1980). They noted a shift in period within the 24–32 mHz range on time scales of ~1500 s. Most of the power in our data is at 31–32 mHz. We will refer to this oscillation as the 32 s oscillation.

The 12 s and 32 s oscillations are both transient. Neither is clearly present in run L22, obtained between

FIG. 10.—Cross-correlation functions for the six orbits for which simultaneous X-ray and optical data were obtained. Each orbit consists of ~3000 s of data collected into 10 s bins.

UT 32441 s and UT 36537 s, nor in any of the other optical runs obtained at LSU and MTW on the two nights, except for run L21 which partially overlaps with run L2M. Their absence from the other optical runs suggests that the 12 s and 32 s oscillations both lasted for ≲1 hr. Their appearance during the same optical run might indicate a relationship between the two oscillations. However, the 12 s oscillation is absent from the Mardirossian *et al.* data, casting doubt upon any such relationship.

The power spectra for the individual X-ray orbits are extremely noisy, due to the low X-ray photon flux. Each orbit contains only about 2000 photons. As a result, oscillations with pulsed fractions less than ~15% are not detectable in individual orbit power spectra. In Figure 13, we present the power spectrum derived by summing the individual power spectra for the orbits 1–8. Even in this case, the noise is substantial, but three features are apparent above the noise. Two of these features, at 31.1 and 80.5 mHz, correspond to the 32 s and 12 s optical oscillations.

To test the significance of these features, the distributions of power for the smoothed X-ray and optical power spectra were compared with the expected white noise distribution,

$$p_N(P > P_0) = \sum_{i=0}^{N-1} [(P_0/P)^i/i!]e^{-P_0/\bar{P}} ,$$

where p_N is the probability that the smoothed power at any given frequency will exceed P_0, $\bar{P}$ is the average unsmoothed power per frequency bin, and N is the number of bins used in the smoothing. The distributions of power for the X-ray and optical data sets fit p_N for all N tested ($N = 1, 3, 5, ..., 21$). A randomly generated data set was subjected to identical analysis, and the resulting distribution of smoothed power was compared with p_N. The distribution of power for the random data set also fits this function for all N tested. The real data sets contain substantial low-frequency power and have padded data gaps. To test whether low-frequency leakage can bias the high-frequency power distribution under these conditions, data gaps identical to the real gaps and a large amplitude low frequency sinusoid were applied to the random data set. The resulting power distribution is indistinguishable from the original distribution. We are therefore confident that p_N gives us an accurate estimate for the probability that various features in the power spectra will be produced by noise.

For the 32 s feature in the summed X-ray power spectrum, the probability that it is spurious, as given by p_N, is 1.4×10^{-4}. The probability that the 12 s feature is spurious is 1.9×10^{-4}. Since 983 frequency bins in the power spectrum were tested, the probability that noise will produce a similar feature somewhere in the spectrum is ~0.15. However, the appearance of these features at the frequencies corresponding to the optical oscillations is significant. There is also an apparent feature at $f \sim 107.8$ mHz (9.3 s). The probability of such a feature being produced by noise somewhere in the X-ray
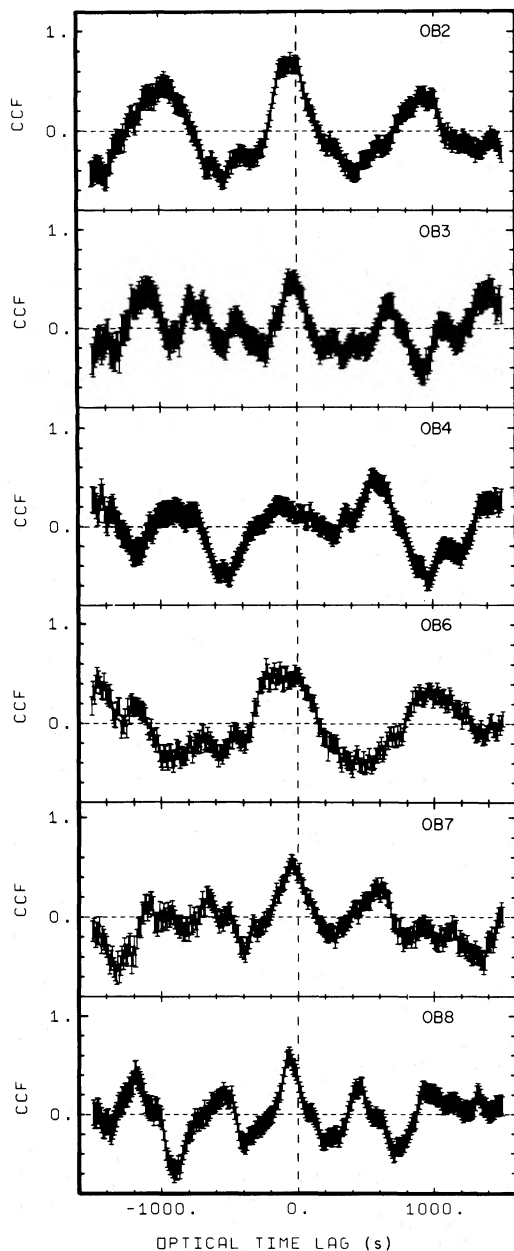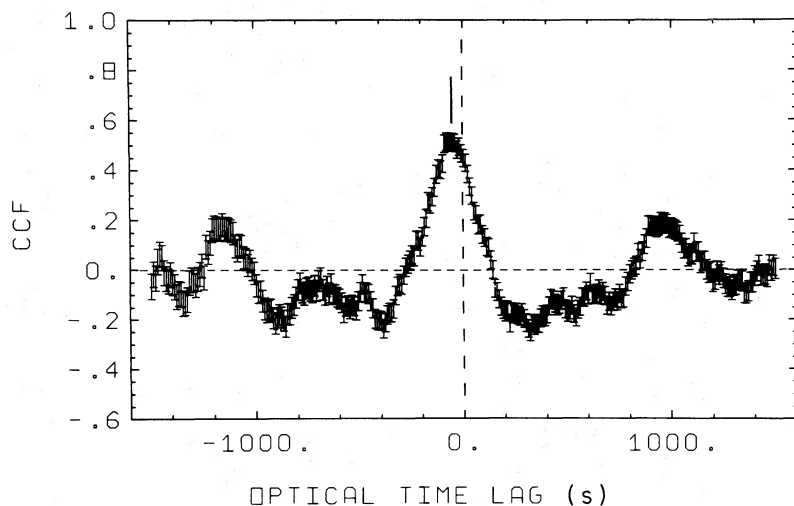
FIG. 11.—Cross-correlation function for the data in orbits 2, 3, 6, 7, and 8. The short vertical bar indicates our best estimate lag of -58 s.
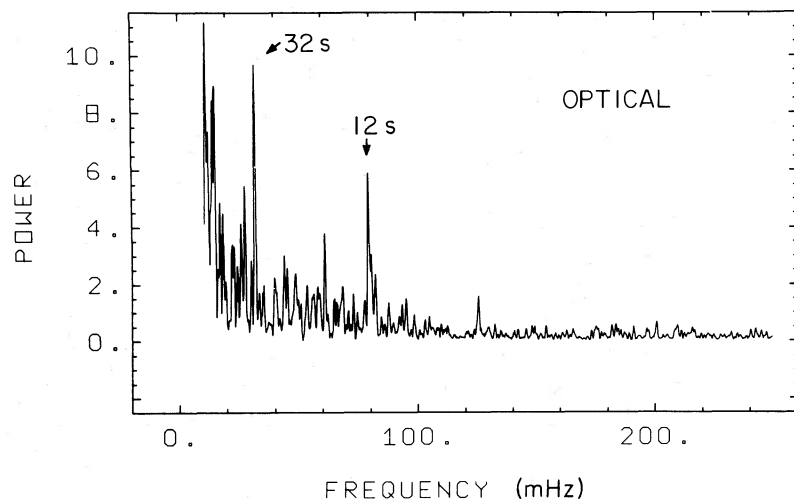

FIG. 12.—The optical power spectrum between 10 and 250 mHz for a 4096 s run (run L2M) obtained on 1980 July 20. The 32 s and 12 s oscillations are indicated. The power spectrum has been smoothed over three bins (0.73 mHz).
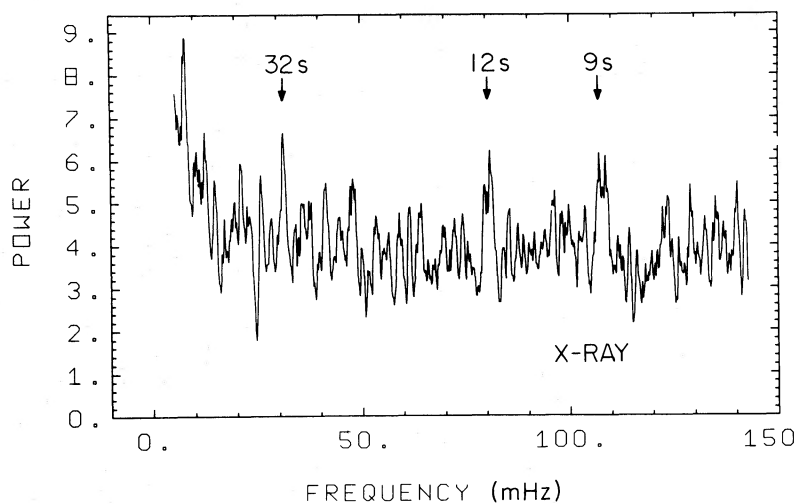

FIG. 13.—The X-ray power spectrum between 5 and 150 mHz derived by summing the power spectra for the eight individual orbits. The 32 s, 12 s, and 9 s features are indicated. The power spectrum has been smoothed over five bins (0.98 mHz).

spectrum is ~ 0.01. This feature and the 12 s oscillation are most prominent for the same orbit (orbit 8). There is no evidence for a corresponding feature in the optical data.

In Table 5, we summarize the characteristics of the rapid oscillations. The frequency spreading (Δf) is determined by the number of bins smoothed for which p_N is minimized, f_0 is the center of the feature at this smoothing, and α is the pulsed fraction summed over Δf, defined as $B_f/\bar{A}$ where the signal is

$$S(t) = A(t) + \sum_{\Delta f} B_f \cos{(2\pi f t)} \ .$$

The pulsed fractions of the X-ray oscillations are 15%–25%; those of the optical oscillations are $\sim 1.5\%$.

It can be seen from Table 5 that $\Delta f/f = 0.02$–0.05 for all of the oscillations. Thus, they are not highly coherent. There are no simultaneous data sets for which we have detectable pulsed fractions for both X-ray and optical oscillations. The oscillations are not sufficiently coherent for an analysis of phase correlations between nonsimultaneous data sets to be feasible.

IV. DISCUSSION

Our simultaneous X-ray and optical observations of TT Ari have revealed several interesting properties:

1. Hard X-ray emission with $kT \gtrsim 10$ keV and an absorbing column density in the range 1–2×10^{21} H atoms cm^{-2}. The ratio of the 0.1–4.0 keV X-ray flux to the 3700–5600 Å optical flux is ~ 0.1.

2. A modulation of the X-ray flux on the same time scale as the probable orbital period of the binary (~ 3.3 hr). The modulated fraction of the X-ray flux is 50%–60%. No associated modulation of the X-ray spectrum is detected.

3. The optical orbital modulation may lag the X-ray modulation by about 0.1 in phase.

4. An X-ray photoelectric absorption event with a duration of ~ 1000 s, and an associated optical event of shorter duration (~ 500 s).

5. Large amplitude X-ray flickering which persists for the entire observation, is present at all orbital phases, and is correlated with optical flickering. The flickering time scale is about 1000 s. The X-ray flickering accounts for 70%–100% of the total X-ray flux. The optical flickering accounts for 15%–20% of the total optical flux.

6. A time delay of 60 ± 20 s between the optical flickering and the X-ray flickering with the optical variability *preceding* the X-ray variability.

7. Rapid optical oscillations which are transient and quasi-periodic are observed with periods of ~ 12 s and ~ 32 s. Hard X-ray oscillations with periods similar to the optical oscillations are also detected. The pulsed fractions of the optical oscillations are between 1.5% and 2%, while the X-ray pulsed fractions are between 15% and 25%.

We now discuss the implications of these results in more detail.

a) The Orbital Modulation

The residual X-ray intensity at minimum phases indicates that the modulation is not caused by a total occultation of a single X-ray emitting source.

The optical modulation, though possibly out of phase with the X-ray modulation, is similar to it in period and modulated fraction and has a similar shape, suggesting that the X-ray and optical modulations are related. This casts doubt upon the idea that the optical modulation is caused by a phase-dependent change in the appearance of an outer disk hot spot, since it is unlikely that 10 keV X-rays can be produced in the outer disk.

TABLE 5
PULSED FRACTIONS FOR THE RAPID OSCILLATIONS

RUN NO.	32 SECOND OSCILLATION			12 SECOND OSCILLATION			9 SECOND OSCILLATION		
	f_0 (mHz)	Δf (mHz)	α (%)	f_0 (mHz)	Δf (mHz)	α (%)	f_0 (mHz)	Δf (mHz)	α (%)
XOB1	31.1	1.4	<9.8	80.5	3.3	17.9 ± 4.8	107.8	2.5	<20.2
XOB2	31.1	1.4	<12.8	80.5	3.3	<8.0	107.8	2.5	<14.9
XOB3	31.1	1.4	15.2 ± 5.1	80.5	3.3	<24.2	107.8	2.5	<9.9
XOB4	31.1	1.4	<22.4	80.5	3.3	<20.8	107.8	2.5	<23.2
XOB5	31.1	1.4	20.7 ± 4.4	80.5	3.3	<18.9	107.8	2.5	16.5 ± 4.3
XOB6	31.1	1.4	<11.0	80.5	3.3	<8.9	107.8	2.5	<8.9
XOB7	31.1	1.4	13.8 ± 4.5	80.5	3.3	<8.8	107.8	2.5	<8.7
XOB8	31.1	1.4	<10.7	80.5	3.3	22.0 ± 3.8	107.8	2.5	22.2 ± 3.7
L11	31.5	0.7	<0.42	80.6	3.7	<0.68	107.9	2.5	<0.23
L12	31.5	0.7	<0.67	80.6	3.7	<0.41	107.9	2.5	<0.15
M11	31.5	0.7	<0.15	80.6	3.7	<0.08	107.9	2.5	<0.08
M12	31.5	0.7	<0.50	80.6	3.7	<0.24	107.9	2.5	<0.13
L21	31.5	0.7	1.34 ± 0.39	80.6	3.7	1.61 ± 0.25	107.9	2.5	<0.42
L2M	31.5	0.7	1.49 ± 0.36	80.6	3.7	1.78 ± 0.21	107.9	2.5	<0.35
L22	31.5	0.7	<0.41	80.6	3.7	<0.62	107.9	2.5	<0.20
M21	31.5	0.7	<0.46	80.6	3.7	<0.30	107.9	2.5	<0.32
M22	31.5	0.7	<0.17	80.6	3.7	<0.08	107.9	2.5	<0.07

Since there is no indication that the X-ray spectrum is modulated, it is unlikely that the orbital modulation of the X-ray flux is caused by photoelectric absorption. The 1000 s absorption event during orbit 4 resulted in an intensity decrease of approximately the same amount as the orbital modulation, and this event produced a clear spectral hardening. If the orbital modulation were due to a similar effect, it would be at least as easy to detect in the spectral data.

The orbital modulation is probably not due to a partial occultation of an inner disk region, since an occultation by an outer disk bulge or by the companion star is difficult to reconcile with the presumed low inclination of the system ($i = 23°$: Warner 1976). Systematic errors in K_w due to asymmetric Balmer lines could have resulted in an underestimate of the inclination, but it is nevertheless unlikely that the inclination can be higher than $\sim 35°$ (Wargau et al. 1982).

The lack of spectral modulation can be understood if the orbital modulation is caused by phase dependent Thomson scattering by electrons. A possible source of electrons may be an expanding wind from the accretion disk. Ultraviolet spectra of TT Ari taken when it was in its bright state have deep, short wavelength shifted ultraviolet absorption lines (Guinan and Sion 1981; Krautter et al. 1981b), suggesting that such a wind exists.

b) The Flickering

Since X-ray flickering accounts for 70%–100% of the total X-ray flux, the 40%–50% orbital modulation is unlikely to be a complete eclipse of a flickering source. This conclusion is supported by the presence of flickering at all orbital phases. A corollary is that the modulation cannot be due to a total eclipse of a steady X-ray source, since such a source can account for $\lesssim 30\%$ of the total intensity. It is more probable that there is a single X-ray emitting region which is dominated by flickering and is partially modulated during the orbital cycle.

The hard spectrum of the X-rays argues that they are not produced in the outer part of an accretion disk. Thus, the correlation in the X-ray and optical flickering suggests that optical flickering may occur in the inner accretion disk. Córdova and Mason (1983) came to a similar conclusion based on observations of X-ray flickering in several cataclysmic variables, on time scales similar to the optical flickering.

Since $L_x/L_B \sim 0.5$ for the flickering, it is clear that there is too much energy in the optical flickering for it to be the low-energy tail of a $kT \gtrsim 10$ keV X-ray flickering component. Barring nonthermal radiation mechanisms, the optical flickering must occur in a region of much lower temperature than does the X-ray flickering, so that flickering is observed from two distinct temperature regions.

These results can be understood if the optical flickering in TT Ari is primarily produced by dissipation of energy in the inner accretion disk, with a fraction of this energy transported to a different region where the X-ray flickering is produced. The time delay between the optical and X-ray flickering would then represent the time required to transport this energy from the optical flickering region to the X-ray emitting region plus the time required for the latter region to respond to the energy input by radiating X-rays. A model for this energy transport is suggested in the following section (§ IVc).

c) Models

Pringle (1977), Pringle and Savonije (1979), and Tylenda (1981) have investigated the possibility of X-ray emission from an equatorial boundary layer which is expected to be formed at the interface between the white dwarf surface and the accretion disk, and where the rapidly rotating accretion disk material is slowed to the white dwarf's rotation rate. The model of Pringle (1977) applies to an optically thick boundary layer, which will be a source of EUV and soft X-ray emission. Since TT Ari is a hard X-ray source, an optically thin boundary layer model would have to be applicable. In Tylenda's model, rotational energy is dissipated by turbulent viscosity. Under the right conditions of mass accretion rate and shear viscosity, a hot ($kT = 1-30$ keV) optically thin plasma can be produced in the vicinity of the boundary layer.

It is difficult to explain how optical and X-ray flickering can be correlated if this model applies to TT Ari. The boundary layer will be a region of strong viscous shearing. A signal from an optically flickering region in the disk is unlikely to be transported radially inward across the shear to the boundary layer. The high degree of correlation between the optical and X-ray flickering suggests a more efficient transport process between the two regions. If we attempt to locate both X-ray and optical flickering in the boundary layer, we have difficulty in explaining the time lag of ~ 1 minute, since the time scales for adiabatic expansion and radiative cooling are on the order of 1 s for the boundary layer densities and temperatures derived by Tylenda. In addition, since $L_x/L_B \sim 0.5$ for the flickering, the optical cannot be a low-energy tail of the X-ray flickering, but rather must be produced in a different region with a lower temperature. The long time lag and the sense of the lag (optical preceding X-ray) rules out reprocessed X-ray flickering as the source of the optical flickering. An additional difficulty with a boundary layer model is that it requires a ratio of hard X-ray luminosity to disk luminosity near unity, since the boundary layer luminosity will be approximately equal to the disk luminosity. Assuming $L_B/L_{disk} \sim 0.1$, TT Ari has a ratio $L_x/L_{disk} \sim 0.01$.

As an alternative, we suggest that the hard X-rays observed from TT Ari may be produced in a hot corona above and below an optically thick inner disk and boundary layer region. If a sufficient fraction of the energy dissipated in this region can be transported vertically out of the disk plane, it may be possible to heat a corona. Icke (1976) suggested that a significant isotropic acoustic flux could be produced if dissipation of rotational energy is achieved by turbulent viscosity.

As the acoustic waves propagate vertically out of the disk plane, the rapidly decreasing gas density results in a steepening into shock waves. Icke suggested that dissipation of these shock waves may serve to heat a disk corona. Liang and Price (1977) suggested an analogy between the generation of the solar corona and an accretion disk corona, in which a turbulent accretion disk plays a role similar to the turbulent solar convection zone as a source of mechanical energy. Galeev, Rosner, and Vaiana (1979) extended this analogy by suggesting that magnetic fields embedded in the disk may be amplified by a differential rotation/convection dynamo, producing magnetic structures in the corona. Closed structures could be the source of hard X-ray emission.

The development of these ideas is similar to the development of our understanding of the solar corona (Vaiana and Rosner 1978; Kuperus, Ionson, and Spicer 1981). The essential picture is that turbulence in the solar convection zone generates an acoustic flux and amplifies small-scale magnetic fields via a rotation/convection dynamo (Parker 1970). The amplified fields produce closed coronal structures (loops) and open coronal structures (holes). As the acoustic waves travel upward toward the chromosphere, the plasma pressure rapidly decreases so that the acoustic modes can couple to magnetohydrodynamic modes, which can transport energy out of the chromosphere into the corona along coronal field lines. Energy transported into coronal loops is liberated by radiative cooling in the loop, producing X-rays. Energy transported into coronal holes is carried away by the solar wind.

A coronal model for the hard X-ray emission from TT Ari can explain many of our observations. The low L_x/L_B ratio can be understood if only a small fraction of the energy dissipated in the accretion disk is transported to the corona. The similarity in the X-ray and optical orbital flux modulations and the lack of X-ray spectral modulation may be explained if the orbital flux modulation is caused by phase-dependent Thomson scattering by electrons in an asymmetric accretion disk wind. A search for evidence of phase-dependent changes in the profiles of the ultraviolet absorption lines in TT Ari is desirable to test this idea. The correlation in the X-ray and optical flickering can be understood as due to the efficiency of acoustic and magnetohydrodynamic transport processes from the disk to the corona.

Since the volume of the corona can be much greater than the volume of the boundary layer, the electron density in the corona can be much less than that required in a hard X-ray boundary layer for a given emission measure. As a result, radiative cooling time scales of ~ 1 minute are possible and may account for the time delay in the X-ray flickering. Radiative cooling will be dominated by free-free emission, since line cooling and recombination are unimportant at the temperature of the X-ray source in TT Ari ($T \gtrsim 10^8$ K). A cooling time scale of 1 minute therefore requires an electron density $n_e = 3 \times 10^{13} \times (T/10^8 \text{ K})^{1/2} \text{ cm}^{-3}$.

The presence of short wavelength shifted absorption lines in the ultraviolet spectrum of TT Ari suggests that vertical energy transport is occurring and that TT Ari exhibits a wind as well as hard X-ray emission. This situation is compatible with the idea that TT Ari has a hot, structured corona produced by turbulent convection in an optically thick inner disk-boundary layer region. The question of whether the processes which produce the solar corona can also produce an accretion disk corona requires further investigation. Similar observations of other cataclysmic variables are also desirable to determine whether the interesting properties we have observed for TT Ari are common among these systems.

REFERENCES

Córdova, F. A., and Mason, K. O. 1983, to be submitted.
Córdova, F. A., Mason, K. O., and Nelson, J. E. 1981, *Ap. J.*, **245**, 609.
Cowley, A. P., Crampton, D., Hutchings, J. B., and Marlborough, J. M. 1975, *Ap. J.*, **195**, 413.
Galeev, A. A., Rosner, R., and Vaiana, G. S. 1979 *Ap. J.*, **229**, 318.
Giacconi, R., *et al.* 1979, *Ap. J.*, **230**, 540.
Grauer, A. D., and Bond, H. 1981, *Pub. A.S.P.*, **93**, 388.
Guinan, E. F., and Sion, E. M. 1981, in The Universe at Ultraviolet Wavelengths: The Second Year of IUE, ed. R. D. Chapman, NASA CP 2171, p. 477.
Harnden, F. R. 1982, Center for Astrophysics Memorandum, November 17.

Icke, V. 1976, in *IAU Symposium 73, The Structure and Evolution of Close Binaries*, ed. P. Eggleton, S. Mitton, and J. Whelan (Dordrecht: Reidel), p. 267.
Krautter, J., Klare, G., Wolf, B., Wargau, W., Dreschel, H., Rahe, J., and Vogt, N. 1981a, *Astr. Ap.*, **98**, 27.
Krautter, J., Klare, G., Wolf, B., Duerbeck, H. W., Rahe, J., Vogt, N., and Wargau, W. 1981b, *Astr. Ap.*, **102**, 337.
Kuperus, M., Ionson, J. A., and Spicer, D. S. 1981, *Ann. Rev. Astr. Ap.*, **19**, 7.
Liang, E. P. T., and Price, R. H. 1977, *Ap. J.*, **218**, 247.
Mardirossian, F., Mezzetti, M., Pucillo, M., Santin, P., Sedmak, G., and Giuricin, G. 1980, *Astr. Ap.*, **85**, 29.

Mattei, J., and Bortle, J. 1982, *IAU Circ.*, No. 3716.
Parker, E. N. 1970, *Ap. J.*, **162**, 665.
Pringle, J. E. 1977, *M.N.R.A.S.*, **178**, 195.
Pringle, J. E., and Savonije, G. J. 1979, *M.N.R.A.S.*, **187**, 777.
Shafter, A., Nolthenius, R., Patterson, J., Bond, H. E., Grauer, A. D., Szkody, P., and Kemper, E. 1982, *IAU Circ.*, No. 3748.
Smak, J., and Stępień, K. 1969, in *Non-Periodic Phenomena in Variable Stars*, ed. L. Detre (Budapest: Academic Press), p. 335.
———. 1975, *Acta Astr.*, **25**, 379.
Tylenda, R. 1981, *Acta Astr.*, **31**, 127.

Vaiana, G. S., and Rosner, R. 1978, *Ann. Rev. Astr. Ap.*, **16**, 393.
Wargau, W., Drechsel, H., Rahe, J., and Vogt, N. 1982, *Astr. Ap.*, **110**, 281.
Warner, B. 1976, in *IAU Symposium 73, The Structure and Evolution of Close Binaries*, ed. P. Eggleton, S. Mitton, and J. Whelan (Dordrecht: Reidel), p. 85.
Weisskopf, M. C., Kahn, S. M., and Sutherland, P. G. 1975, *Ap. J. (Letters)*, **199**, L147.
Williams, J. O. 1966, *Pub. A.S.P.*, **78**, 279.

F. A. Córdova and J. Middleditch: ESS-9, MS D436, Los Alamos National Laboratory, Los Alamos, NM   87545

R. Gomer: Department of Biology, 156-29, California Institute of Technology, Pasadena, CA   91125

A. D. Grauer: Department of Physics and Astronomy, University of Arkansas at Little Rock, 33rd Street and University, Little Rock, AR   72204

K. Horne: Department of Astronomy, 105-24, California Institute of Technology, Pasadena, CA 91125

K. A. Jensen: Laboratory for High Energy Astrophysics, Goddard Space Flight Center, Code 661, Greenbelt, MD   20771

K. O. Mason: Mullard Space Science Laboratory, Holmbury St. Mary, Nr. Dorking, Surrey, RH5 6NT, England, U.K.